Atmospheric Environment 214 (2019) 116817

Contents lists available at ScienceDirect

Atmospheric Environment

journal homepage: www.elsevier.com/locate/atmosenv

A model investigation into the atmospheric NO_y chemistry in remote continental Asia

K.M. Han[a,b], S. Lee[a,b,c], Y.J. Yoon[d], B.Y. Lee[d], C.H. Song[a,b,*]

[a] School of Earth Sciences and Environmental Engineering, Gwangju Institute of Science and Technology (GIST), Gwangju, 61005, South Korea
[b] Center for Earth and Environmental Modeling Studies (CEMOS), Gwangju Institute of Science and Technology (GIST), Gwangju, 61005, South Korea
[c] Department of Earth and Atmospheric Sciences, University of Houston, Houston, TX, 77204, USA
[d] Division of Polar Climate Science, Korea Polar Research Institute (KOPRI), Incheon, 21990, South Korea

GRAPHICAL ABSTRACT

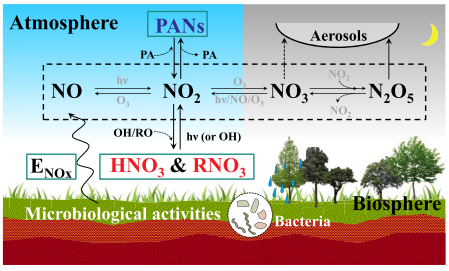

ARTICLE INFO

Keywords:
Tropospheric NO_2 column
Columnar net NO_x chemical production rates ($\bar{P}_{NOx}$)
Thermal decomposition of PANs
NO_x chemical loss
Soil NO_x emissions
OMI

ABSTRACT

The OMI-observed tropospheric NO_2 columns over highly polluted regions in East Asia showed high values during the cold seasons and low values during the warm seasons. On the contrary, the monthly trends over Mongolia are completely opposite to those in polluted regions in East Asia. This study was initiated by such an interesting contrast. To determine the key factors controlling such monthly trends over Mongolia, we used the WRF-CMAQ simulated data. In the analysis, we explored the budget of $\bar{P}_{NOx}$ (columnar net NO_x chemical production rates), taking into account atmospheric chemical production and removal of NO_x as well as surface (soil) NO_x emissions. For the polluted regions, NO_x emissions show the largest values, followed by $\bar{P}_{RNO3}$in terms of the magnitudes. Among the negative contributors, the largest contribution is made by $\bar{P}_{RNO3}$ (columnar net NO_x chemical production rates via the HNO_3 and RNO_3-related reactions) ranging between −42% and −77% during the warm months. Other negative contributions from $\bar{P}_{PANs}$(columnar net NO_x chemical production rates via the formations and decompositions of PANs) and $\bar{P}_{Hetero.}$(columnar net NO_x chemical production rates via the heterogeneous reactions of NO_3 and N_2O_5) are relatively small. Unlike the situations over the polluted regions, the negative $\bar{P}_{RNO3}$ was offset completely by E_{NOx} (emission of NO_x) and positive $\bar{P}_{PANs}$over the remote continental regions of Mongolia. $\bar{P}_{PANs}$ was also regarded as an important atmospheric process, and its positive contributions range between 5% and 51% over the remote continental regions of (south) Mongolia. From the analysis, it was found that NO_2 produced via thermal decomposition of PANs in the remote continental regions of Mongolia contribute to the high NO_2 columns during the warm seasons and low values during the cold seasons.

* Corresponding author. School of Earth Sciences and Environmental Engineering, Gwangju Institute of Science and Technology (GIST), Gwangju, 61005, South Korea.
E-mail address: chsong@gist.ac.kr (C.H. Song).

https://doi.org/10.1016/j.atmosenv.2019.116817
Received 27 November 2018; Received in revised form 26 June 2019; Accepted 1 July 2019
Available online 03 July 2019
1352-2310/

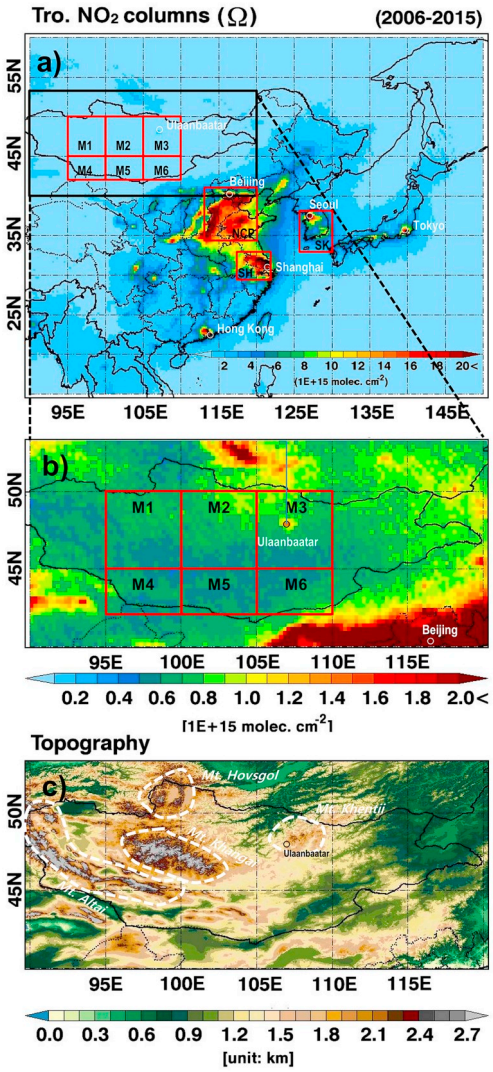

Fig. 1. OMI-retrieved tropospheric NO_2 columns averaged between January 2006 and December 2015 over a) East Asia, and b) Mongolia. Detailed analysis regions of M1, M2, M3, M4, M5, M6, NCP, SH, and SK. c) Topography and permafrost areas (Khangai, Altai, Hovsgaol, and Khentii Mountains) in Mongolia.

1. Introduction

Ulaanbaatar, the capital city of Mongolia, has been reported to be one of the most polluted cities in the world (WHO, 2014, 2016). Many studies carried out in Ulaanbaatar reported that the severe air pollution is caused by the combination of man-made pollution with topographic and stable meteorological effects, particularly during the cold seasons (Davy et al., 2011; Batmunkh et al., 2013; Huang et al., 2013). In Ulaanbaatar, anthropogenic pollutants are mainly emitted by internal combustion vehicles, coal-fired power plants, and coal/wood-based traditional dwelling systems (World Bank, 2009).

On the contrary, remote regions of Mongolia, which occupy most parts of the country, can be said to have good air quality. In these regions, it has been reported that NO_x is mainly emitted from microbiological processes in soils (Yienger and Levy, 1995; Vinken et al., 2014). NO_x can be one of the key factors controlling atmospheric chemistry in the remote continental regions (Jaeglé et al., 2004). NO_x is also potentially released from permafrost soils distributed in some areas of Mongolia (see Fig. 1(c)), because the temperatures in the areas have risen rapidly over the last 30 years (Sharkhuu, 2003).

Despite its importance, limited *in situ* ground measurements have been conducted in these regions. Only ~40 air quality monitoring stations are currently under operation. Twelve of these stations are located in the capital city, Ulaanbaatar (http://www.air.ub.gov.mn/en/about/station-map.html). Unfortunately, it is difficult to obtain the official air quality data of Mongolia.

On the contrary, space-borne observations from the Global Ozone Monitoring Instrument (GOME), GOME II, SCanning Image Absorption spectroMeter for atmospheric CHartographY (SCIAMACHY), and Ozone Monitoring Instrument (OMI) can be an alternative tool for analyzing spatial and temporal variations of air pollutants over the wide areas of Mongolia (refer to Fig. 1).

Recently, several studies have analyzed the seasonal and annual trends of tropospheric NO_2 columns retrieved from the OMI and SCIAMACHY sensors for decades, specifically in the polluted regions (Schneider et al., 2015; de Foy et al., 2016; Duncan et al., 2016; Krotkov et al., 2016). However, long-term analysis of tropospheric NO_2 columns has not been frequently carried out for the remote continental regions. Analysis for the remote continental regions is essential for one to understand the atmospheric chemistries in the background regions of the Earth.

Monthly variations of tropospheric NO_2 columns over the remote continental regions show an opposite trend to those over polluted regions. In polluted regions, the tropospheric NO_2 columns are highest during winter, and lowest during summer. On the contrary, the tropospheric NO_2 columns in the remote continental regions are highest during summer, and are lowest during winter as shown in Fig. 2. Similar monthly trends have also been found in other remote regions such as the western parts of China, North America, and Northern Europe (van der A et al., 2006; 2008). This is an interesting trend worth investigating.

Therefore, the objective of this study is to investigate this trend shown in the monthly variations of tropospheric NO_2 columns in the remote continental regions of Asia (Mongolia). We analyzed OMI-observed tropospheric NO_2 columns from 2006 to 2015, which were retrieved via the KNMI/DOMINO v2.0 algorithm (refer to Sect. 2.1). Also, the Community Multi-scale Air Quality (CMAQ)/Weather Research and Forecasting (WRF) model simulations were carried out to thoroughly examine what process(es) actually control(s) such monthly trends of tropospheric NO_2 columns from the OMI observations. In this study, we

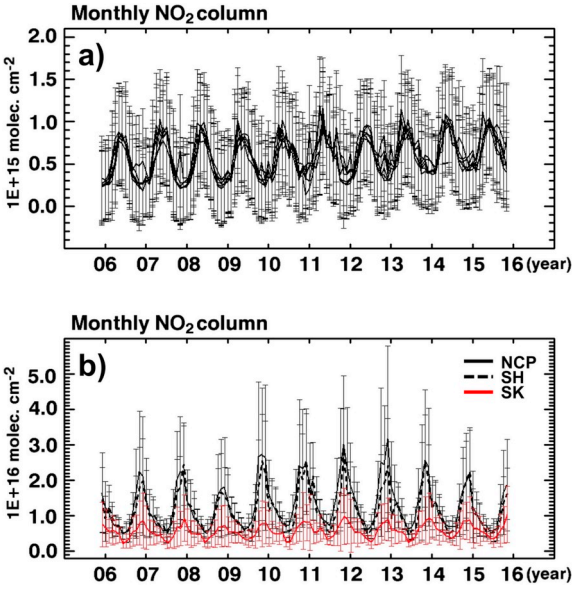

Fig. 2. Monthly variations of OMI-retrieved tropospheric NO_2 columns (with error bars) from January 2006 to December 2015 over (a) six analysis regions (i.e. M1 to M6 defined in Fig. 3) in Mongolia, and (b) North China Plain (NCP), Shanghai (SH), and South Korea (SK) regions.

probed into several atmospheric processes that could be responsible for the monthly trends of tropospheric NO_2 columns over Mongolia. This will be intensively discussed in Sects. 3.3 and 3.4.

2. Methods

2.1. OMI observations

Since October 2004, the OMI sensor on board the NASA/EOS-Aura satellite has provided global-scale information on the atmospheric air pollutants with a spatial resolution of 13 km × 24 km at the nadir (Levelt et al., 2006). The OMI sensor has an overpass time of approximate 13:45 local time (LT), and covers the globe in one day. We used the tropospheric NO_2 columns (hereafter, denoted by Ω_{OMI}) retrieved from the OMI instrument for a decadal (2006–2015) analysis of Mongolia. The level-2 products from the KNMI/DOMINO v2.0 algorithm (Boersma et al., 2011a, 2011b) were obtained from the website of the Tropospheric Emission Monitoring Internet Service (TEMIS, www.temis.nl). The DOMINO v2.0 products used in this study have been validated and used in many field studies (Irie et al., 2012; Mendolia et al., 2013; Lin et al., 2014; Boersma et al., 2015; Shaiganfar et al., 2015; Jin et al., 2016).

The daily tropospheric NO_2 columns were generally retrieved in a three-step procedure: i) NO_2 slant columns were obtained from the OMI reflectance spectra using the Differential Optical Absorption Spectroscopy (DOAS) method; ii) The tropospheric contribution of the NO_2 slant columns was estimated; and iii) The tropospheric NO_2 slant columns were converted to tropospheric NO_2 vertical columns using the air mass factor (AMF). In this study, we re-gridded the daily data into a regular 0.25° × 0.25° grid. Monthly averages of tropospheric NO_2 columns of Mongolia were then calculated on a daily basis.

In the retrieval, the errors in the tropospheric NO_2 columns are mainly caused by the calculations of the AMF, which is a function of the *a priori* profile, cloud, surface albedo, surface pressure, and terrain height (Boersma et al., 2011a). To reduce the retrieval errors, the scenes contaminated by clouds (cloud radiance fraction > 0.5) and bright surfaces (surface albedo > 0.3) were discarded, as recommended by Boersma et al. (2011b). The total errors in the tropospheric NO_2 columns ranged from 4.87×10^{14} to 6.16×10^{14} molecules cm^{-2} over the selected areas of Mongolia. We have recognized that the values of tropospheric NO_2 columns over the remote parts of Mongolia are rather close to the detection limit (~2×10^{14} molecules cm^{-2}) of the OMI NO_2 remote sensing. However, in Mongolia (or remote continental regions), meaningful *in situ* observation data is hardly available, which is the main reason as to why this study uses tropospheric NO_2 columns.

2.2. CMAQ model simulations

To determine what processes control the trend of tropospheric NO_2 columns over Mongolia, the WRF-CMAQ model simulations were performed for the year, 2010. The CMAQ v4.7 model simulations produced data with 30km × 30 km horizontal resolution and with 14 vertical levels (Byun and Schere, 2006). The CMAQ v4.7 model was driven by meteorological fields generated from the WRF v3.4.1 model (Skamarock et al., 2008).

Main physical schemes employed in the WRF v3.4.1 model simulations were Yonsei University (YSU) scheme for the planetary boundary layer (Hong et al., 2006), Rapid Radiative Transfer Model (RRTM) scheme for the long-wave radiation (Mlawer et al., 1997), and Dudhia scheme for the shortwave radiation (Dudhia, 1989). For the CMAQ v4.7 model simulations, anthropogenic, biogenic, and fire emissions were obtained from the Model Inter-comparison Study for Asia Phase III (MICS-Asia III; Li et al., 2017), Model of Emission of Gases and Aerosols from Nature-Monitoring Atmospheric Composition and Climate (MEGAN-MACC; Sindelarova et al., 2014) and Quick Fire Emissions Database version 2.4 (QFED v2.4; Darmenov and da Silva, 2013), respectively. Natural NO_x emissions as a result of microbiological processes in soils obtained from the REAS v2.1 inventory were also used in the CMAQ v4.7 model simulations (Kurokawa et al., 2013).

The chemical mechanism employed in the CMAQ v4.7 simulations was the Statewide Air Pollution Research Center-99 (Carter, 2000). For the consideration of aerosol dynamic and thermodynamics, AERO 4 module was also used (Binkowski and Rosell, 2003). The chemical boundary conditions were taken from the outputs of Model for Ozone and Related Chemical Tracers, version 4 (MOZART-4) model simulations (http://www.acom.ucar.edu/wrf-chem/mozart.shtml). For the chemical mapping of VOC species in MOZART-4 to those in SAPRC-99 scheme, we followed a method recommended by Emmons et al. (2010).

For direct comparison analysis, the CMAQ-calculated NO_2 data were collected spatially and temporally at the scanning time of OMI observations (i.e. approximate 13:30 local time). For the monthly budget analysis, all chemical and meteorological data calculated from the WRF-CMAQ model simulations were extracted on an hourly basis.

3. Results and discussions

3.1. Modeling performance

In order to examine the WRF-CMAQ model performances in North-East Asia, we compared the simulated concentrations with observed concentrations. First, ground-based observation data of nitrate (NO_3^-), ammonium (NH_4^+), HNO_3, and ozone were collected from the Acid Deposition Monitoring Network in East Asia (EANET, 2012). In Fig. 3, monthly-averaged concentrations of the gaseous and particulate species from the CMAQ model simulations (gray bars) and the EANET (red circles) were compared for five "remote sites" in East Asia: Terelj (47.98°N, 107.48°E, 1540 m above sea level (a.s.l.)), Mondy (51.67°N, 101.00°E, 2000m a.s.l.), Listvianka (51.85°N, 104.90°E, 700 m a.s.l.), Kangwha (37.70°N, 126.28°E, 150 m a.s.l.), and Cheju (33.30°N, 126.17°E, 72 m a.s.l.). The locations of the remote sites are shown in Fig. S1. In the context of discussing atmospheric NO_y chemistry, it would be more desirable that the concentrations of observed and modeled NO_y species were compared. However, among the NO_y species, HNO_3 and NO_3^- were the only available concentrations from the EANET. For further validation, the comparisons between CMAQ-modeled and OMI-observed NO_2 columns were also made (see Sect. 3.2).

In the remote regions of Terelj and Mondy, relatively low concentrations of gaseous and particulate species were observed (i.e. $[HNO_3] < \sim 2$ ppb; $[NO_3^-]$ and $[NH_4^+] < \sim 1$–$2\ \mu g\ m^{-3}$). Such low values were reasonably well simulated by the CMAQ model simulations. At another monitoring station in Listvianka, the concentrations of HNO_3 and particulate species were comparable to those at the stations in Terelj and Mondy. Such magnitudes of gaseous and particulate species in Listvianka were also captured by the CMAQ model simulations.

Monthly variations of ozone mixing ratios calculated by the CMAQ model were generally consistent with those observed at Kangwha, Mondy, and Cheju stations, although the simulated ozone mixing ratios were higher than those recorded from observations, especially in summer seasons. The overestimation of CMAQ-simulated O_3 would have some impacts on the NO-to-NO_2 ratios and NO_x lifetimes. As mentioned previously, satellite-retrieved NO_2 columns were also compared with the CMAQ-calculated NO_2 columns for further model validation in Sect. 3.2.

3.2. Spatial and temporal trends of tropospheric NO_2 columns over Mongolia

In this section, tropospheric NO_2 columns over Mongolia and some polluted areas from OMI sensor (Ω_{OMI}) were analyzed. Fig. 1(a) shows the spatial distributions of the average Ω_{OMI} over East Asia between

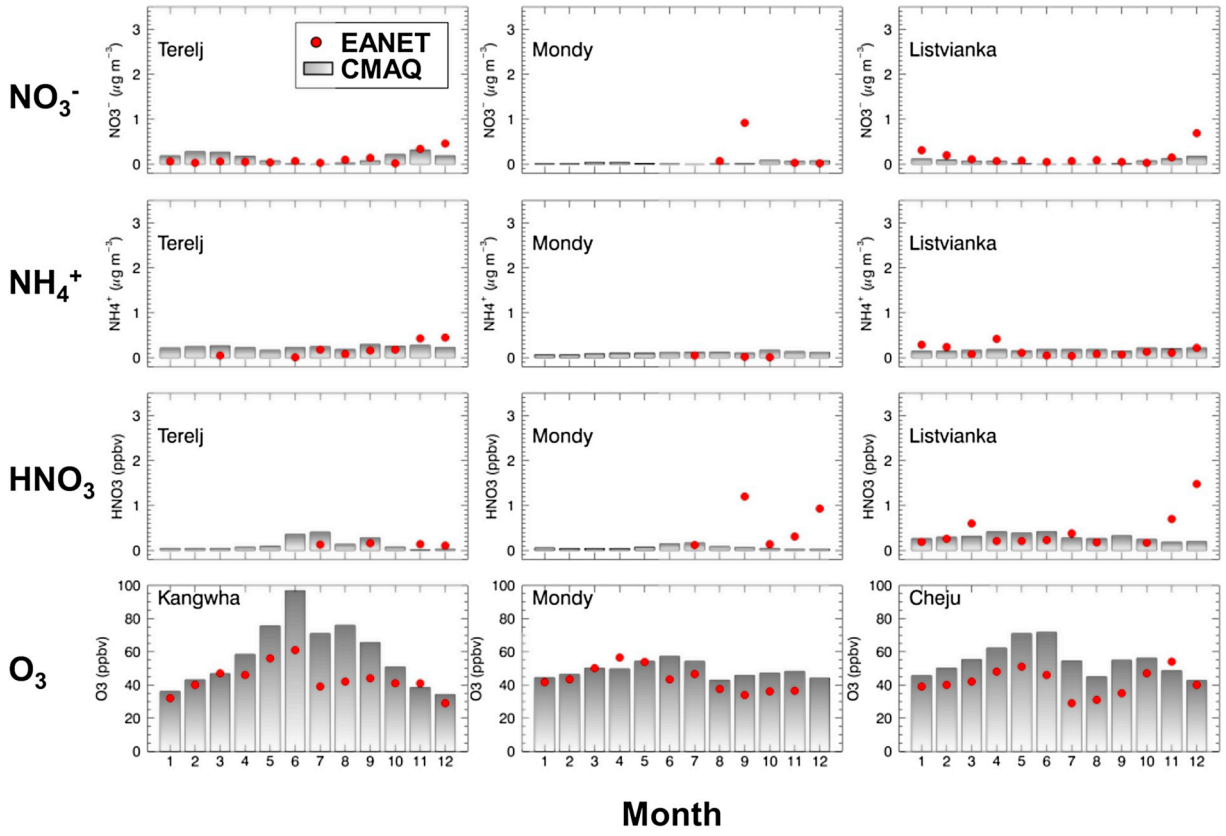

Fig. 3. Monthly averaged concentrations of nitrate (1st row), ammonium (2nd row), HNO_3 (3rd row), and O_3 (4th row) from CMAQ model simulations (gray bar) and ground-based measurements (red circle) at several EANET monitoring stations. (For interpretation of the references to colour in this figure legend, the reader is referred to the Web version of this article.)

2006 and 2015. The Ω_{OMI} over Mongolia approximately ranges from 0.5×10^{15} to 1.0×10^{15} molecules cm^{-2}, which are the lowest values in East Asia. In this sense, the atmospheric levels in Mongolia may be considered as continental background levels in East Asia. On the contrary, Fig. 1(b) shows a relatively high peak of Ω_{OMI} around Ulaanbaatar, although the value of $\sim 1.42 \times 10^{15}$ molecules cm^{-2} is still lower than Ω_{OMI} in mega-cities over East Asia, such as Beijing, Shanghai, Hong Kong, Seoul, and Tokyo. Such relatively high values are possibly caused by local effects from anthropogenic sources, such as transportation and power generation in Ulaanbaatar, as introduced in Sect. 1.

Fig. 2(a) shows the average monthly variations of Ω_{OMI} of 6 selected regions for one decade. The three northern (M1, M2, and M3 in Fig. 1) and three southern (M4, M5, and M6 in Fig. 1) regions of Mongolia were chosen for this study because the six regions show somewhat different NO_y characteristics and topographical changes (also, refer to Fig. 1(c)). Fig. 2(a) shows the monthly variations in Ω_{OMI}. The Ω_{OMI} values over Mongolia are higher during the warm seasons and lower during the cold seasons. These trends are opposite to the trends over the North China Plain (NCP), Shanghai (SH) region, and South Korea (SK) as shown in Fig. 2(b). These three polluted regions were chosen for comparison and contrast with Mongolia. Many other studies of 3D-chemistry-transport model simulations and satellite observations have also reported the same phenomena (Richter et al., 2005; van Noije et al., 2006; Boersma et al., 2009; Huijnen et al., 2010; Han et al., 2011, 2015; Lamsal et al., 2014; Choi and Souri, 2015). Typically, satellite-observed NO_2 columns are lower in summer, because the photochemical removal of atmospheric NO_x through the oxidation by OH radicals is most active in summer, hence the shorter lifetimes of NO_x during summer (Lamsal et al., 2010)

We investigated what process(es) actually cause(s) this opposite trend of Ω_{OMI} variation in Mongolia. We used tropospheric NO_2 columns calculated from the WRF-CMAQ model simulations (hereafter, Ω_{CMAQ}). The Ω_{CMAQ} were spatially compared with Ω_{OMI} in Fig. S2 on a monthly basis. In general, it was found that there was good consistency in Ω_{OMI} and Ω_{CMAQ}.

For a more detailed analysis, monthly variations of Ω_{OMI} (with black lines) and Ω_{CMAQ} (with red dotted lines) of the six selected regions for 2010 were plotted together in Fig. 4. For direct comparison between two columns, averaging kernels (AKs) were also applied to the NO_2 columns calculated by CMAQ model simulations. As shown in Fig. 4, the monthly variations of Ω_{CMAQ} and Ω_{OMI} over the remote continental regions of southern Mongolia (M4, M5, and M6) and polluted areas (NCP, SH, and SK) were generally consistent. The index of agreements (IOA) for southern Mongolia ranged from 0.76 to 0.87 and that of polluted areas from 0.71 to 0.89. The IOA is a standard measure for the degree of prediction errors, ranging from 0 to 1 (Willmott, 1981). These results indicate that the CMAQ model simulations successfully reproduce the trends and magnitudes of Ω_{OMI} in (southern) Mongolia and the polluted areas, although the monthly-averaged values of Ω_{CMAQ} were rather lower than those of Ω_{OMI} over the northern parts of Mongolia (M1, M2, and M3 regions). Based on this, we attempted to determine the main factor(s) influencing the monthly trends of Ω_{OMI} in Mongolia using the outputs from the WRF-CMAQ model simulations.

3.3. Net NO_x productions

Using the outputs from the CMAQ model simulations, we investigated the budget of atmospheric NO_x. Although we discuss the trends of the NO_2 columns over Mongolia, we analyzed the formation and destruction of NO_x, because the interconversions among the NO_x species were so fast (e.g. the lifetimes of NO and NO_2 are only several minutes). We considered all photochemical reactions related to the formation and removal of NO_x ($\cong NO + NO_2 + NO_3 + 2N_2O_5$) in the

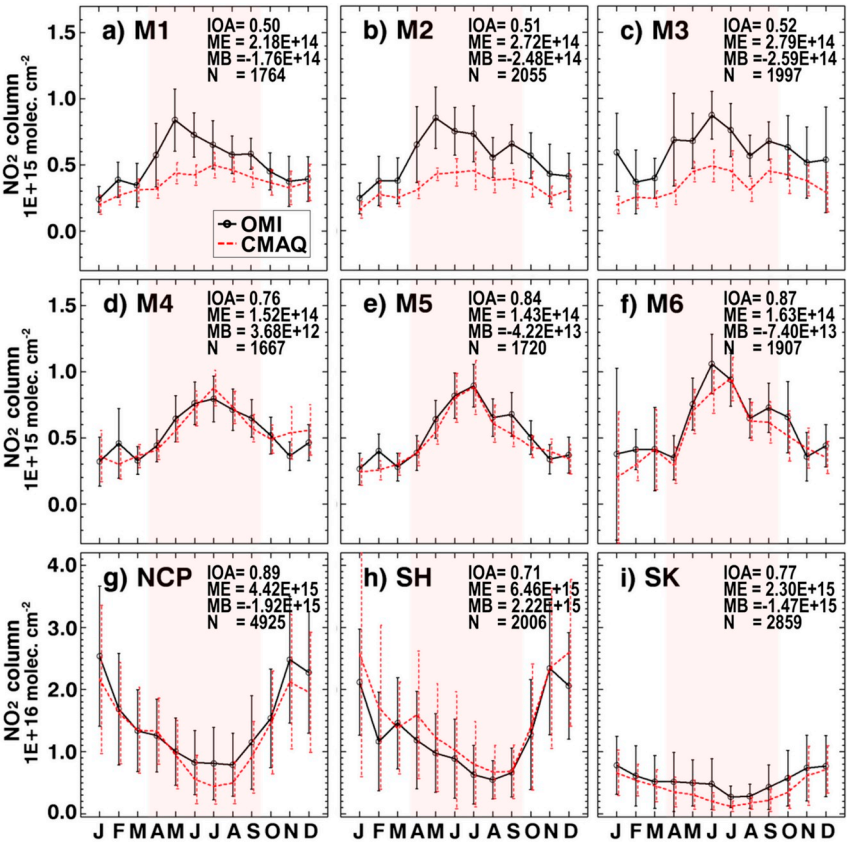

Fig. 4. Monthly variations of tropospheric NO_2 columns over the 9 analysis regions. Black and red lines represent data from OMI sensor and from WRF-CMAQ model simulations for 2010, respectively. Red-shaded areas represent the warm seasons (i.e., April–September) in this study. Panels of g), h), and i) have different scales in y-axis. (For interpretation of the references to colour in this figure legend, the reader is referred to the Web version of this article.)

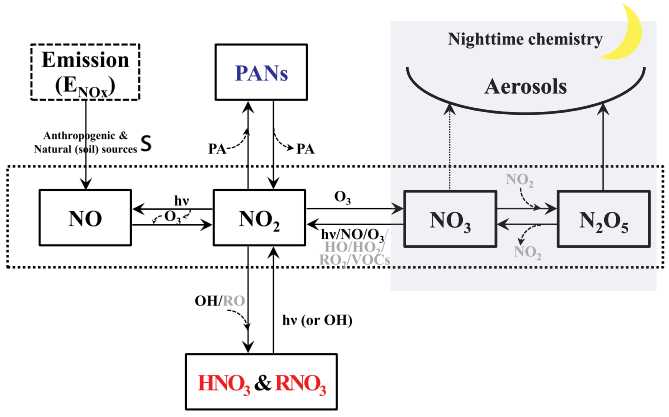

Fig. 5. Illustration of atmospheric NO_y chemistry considered in this study.

SAPRC-99 chemical mechanism as illustrated in Fig. 5. As presented in Table 1 and Fig. 5, the reactions can be classified into five groups. NO_x productions have two groups: i) PANs decomposition (F_{PANs}, reaction 1–4 in Table 1) and ii) HNO_3 and RNO_3-related reactions (F_{RNO3}, reaction 9–12 in Table 1). On the other hand, NO_x is also removed via three reaction channels: i) PANs formations (L_{PANs}, reaction 5–8 in Table 1), ii) HNO_3 and RNO_3 formations (L_{RNO3}, reaction 13–14 in Table 1), and iii) heterogeneous reactions of NO_3 and N_2O_5 onto atmospheric aerosols (L_{hetero}, reaction 15–16 in Table 1). Based on this, NO_x formation (F_{NOx}) and loss (L_{NOx}) rates can be constructed by following Eqs. (1) and (2):

$$\begin{aligned} F_{NOx} &\equiv F_{PANs} + F_{RNO3} \\ &\equiv k_1[PAN] + k_2[PAN2] + k_3[MA\_PAN] + k_4[PBZN] + \\ &\quad j_9[HNO_3] + j_{10}[HONO] + 0.338k_{11}[RNO_3][HO] + j_{12}[RNO_3] \end{aligned} \quad (1)$$

$$\begin{aligned} L_{NOx} &\equiv L_{PANs} + L_{RNO3} + L_{hetero} \\ &\equiv k_5[NO_2][CCO\_O2] + k_6[NO_2][RCO\_O2] + k_7[NO_2][MA\_RCO3] + \\ &\quad k_8[NO_2][BZCO\_O2] + k_{13}[NO_2][HO] + k_{14}[NO_2][TBU\_O] + \\ &\quad 2k_{h,15}[N_2O_5] + k_{h,16}[NO_3] \end{aligned} \quad (2)$$

All the reaction rate coefficients (k_i) were calculated on the basis of the SAPRC-99 chemical mechanism (Carter, 2000). For the calculations of photolysis rate coefficients (j_i) of reactions 9, 10, and 12 in Table 1, clear-sky J-values ($j_{clear\text{-}sky}$) and the photolysis reaction rate coefficients were first extracted from the photolysis rate table (i.e., look-up tables from JPROC processing in CMAQ model simulations) with spatial, temporal, and geographical information (such as heights, latitude and local time) in a given grid cells. Then, we corrected the clear-sky J-values by multiplying correction factors based on model-estimated cloud fractions in the given grid cells (Chang et al., 1987; EPA, 1999). The heterogeneous reaction rate coefficients ($k_{h,i}$) were calculated by Schwartz formula of $k_{h,i} = \gamma_i S \upsilon_i / 4$ (Schwartz, 1986). The reaction probability of N_2O_5 (γ_{N2O5}) was calculated from a combined parameterization of Evans and Jacob (2005) and Riemer et al. (2003), in which the γ_{N2O5} is a function of relative humidity, temperature, and the composition of sulfate and nitrate (Davis et al., 2008). Also, γ_{NO3} was set to 0.01 (Exner et al., 1994; Jacob, 2000). The S and υ_i represent the aerosol surface density ($\mu m^2\ cm^{-3}$) and molecular mean velocity ($cm\ s^{-1}$) for the species, i, respectively. Although both N_2O_5 and NO_3 radicals are known as nighttime species, we took both radicals into consideration because the nighttime processes can also influence the daytime levels of NO_x.

The levels of atmospheric NO_x were determined by the balance between the F_{NOx} and L_{NOx}. The net NO_x chemical production rate, P_{NOx} (unit: molecules $cm^{-3}\ s^{-1}$), is then calculated by Eq. (3):

$$P_{NOx} = F_{NOx} - L_{NOx} \quad (3)$$

We converted P_{NOx} (molecules $cm^{-3}\ s^{-1}$) to the columnar net NO_x chemical production rates ($\bar{P}_{NOx}$, molecules $cm^{-2}\ s^{-1}$) via vertical integrations of P_{NOx} from the surface to approximately 10 km. As

Table 1
Photochemical reactions of SAPRC-99 chemical mechanism used for the budget analysis of NO_x.

Category	Rxn. No.	Reactants		Products	Reaction rates[a)]
F_{PANs}	1	PAN	→	NO2 + CCO_O2	k_0 = 4.90E-03·exp(-12100/T), k_{inf} = 4.00E+16·exp(-13600/T), f = 0.3
	2	PAN2	→	NO2 + RCO_O2	2.00E+15·exp(-12800/T)
	3	MA_PAN	→	NO2 + MA_RCO3	1.60E+15·exp(-13486/T)
	4	PBZN	→	NO2 + BZCO_O2	7.90E+16·exp(-14000/T)
L_{PANs}	5	NO2 + CCO_O2	→	PAN	k_0 = 2.70E-28·(T/300)$^{(-7.10)}$, k_{inf} = 1.21E-11·(T/300)$^{(-0.90)}$, f = 0.3
	6	NO2 + RCO_O2	→	PAN2	1.20E-11·(T/300)$^{(-0.90)}$
	7	NO2 + MA_RCO3	→	MA_PAN	1.20E-11·(T/300)$^{(-0.90)}$
	8	NO2 + BZCO_O2	→	PBZN	1.37E-11
F_{RNO3}	9	HNO3	→	NO2 + HO	Photolysis reaction
	10	HONO	→	NO2 + HO2	Photolysis reaction
	11	RNO3 + HO	→	0.338 × NO2 + 0.113 × HO2 + 0.376 × RO2_R + 0.173 × RO2_N + 0.596 × R2O2 + 0.01 × HCHO + 0.439 × CCHO + 0.213 × RCHO + 0.006 × ACET + 0.177 × MEK + 0.048 × PROD2 + 0.31 × RNO3	7.80E-12
	12	RNO3	→	NO2 + 0.341 × HO2 + 0.564 × RO2_R + 0.095 × RO2_N + 0.152 × R2O2 + 0.134 × HCHO + 0.431 × CCHO + 0.147 × RCHO + 0.02 × ACET + 0.243 × MEK + 0.435 × PROD2	Photolysis reaction
L_{RNO3}	13	NO2 + HO	→	HNO3	k_0 = 2.43E-30·(T/300)$^{(-3.10)}$, k_{inf} = 1.67E-11·(T/300)$^{(-2.10)}$, f = 0.6
	14	NO2 + TBU_O	→	RNO3	2.40E-11
L_{N2O5}	15	N2O5	→	2 × NO_3^-	Heterogeneous reaction rate coefficient ($k_{h,i}$)[b)] γ_{N2O5} (combination of parameterizations from Evans and Jacob (2005) and Riemer et al. (2003)
	16	NO3	→	NO_3^-	Heterogeneous reaction rate coefficient ($k_{h,i}$)[b)] γ_{NO3} = 0.01 (Jacob, 2000)

PAN	: Peroxyacetyl Nitrate	MA_RCO3	: Peroxyacyl radicals formed from methacrolein and other acroleins
PAN2	: PPN and other higher alkyl PAN analogues	BZCO_O2	: Peroxyacyl radical formed from aromatic aldehydes
MA_PAN	: PAN analogue formed from Methacrolein	RNO3	: Lumped organic Nitrates
PBZN	: PAN analogue formed from Aromatic Aldehydes	TBU_O	: t-Butoxy radicals
CCO_O2	: Acetyl Peroxy radicals	HCHO	: Formaldehyde
RCO_O2	: Peroxy Propionyl and higher peroxy acyl radicals	CCHO	: Acetaldehyde
RO2_R	: Peroxy radical operator representing NO to NO2 conversion with HO2 formation	RCHO	: Lumped C3+Aldehydes
		ACET	: Acetone
R2O2	: Peroxy radical operator representing NO to NO2 conversion without HO2 formation	MEK	: Ketones and other non-aldehyde oxygenated products which react with OH radicals slower than 5×10^{-12} cm^3 $molec.^{-2}$ sec^{-1}
RO2_N	: Peroxy radical operator representing NO consumption with organic nitrate formation	PROD2	: Ketones and other non-aldehyde oxygenated products which react with OH radicals faster than 5×10^{-12} cm^3 $molec.^{-2}$ sec^{-1}

[a)] k_0 and k_{inf} represent low- and high-pressure limiting rate constants. For the calculation of reaction rate (k), the parameters of k_o, k_{inf}, and f were fed into the following equation. $k = \frac{k_0[M]}{1+k_0[M]/k_{inf}} f^{\left\{1+\left[\log_{10}\left(\frac{k_0[M]}{k_{int}}\right)\right]^2\right\}^{-1}}$

[b)] γ_{N2O5} and γ_{NO3} represent reaction probabilities of N_2O_5 and NO_3, respectively. The heterogeneous reaction rate coefficients (k_h) were calculated from Schwartz formula, $k_{h,i} = \frac{\gamma_i S v_i}{4}$.

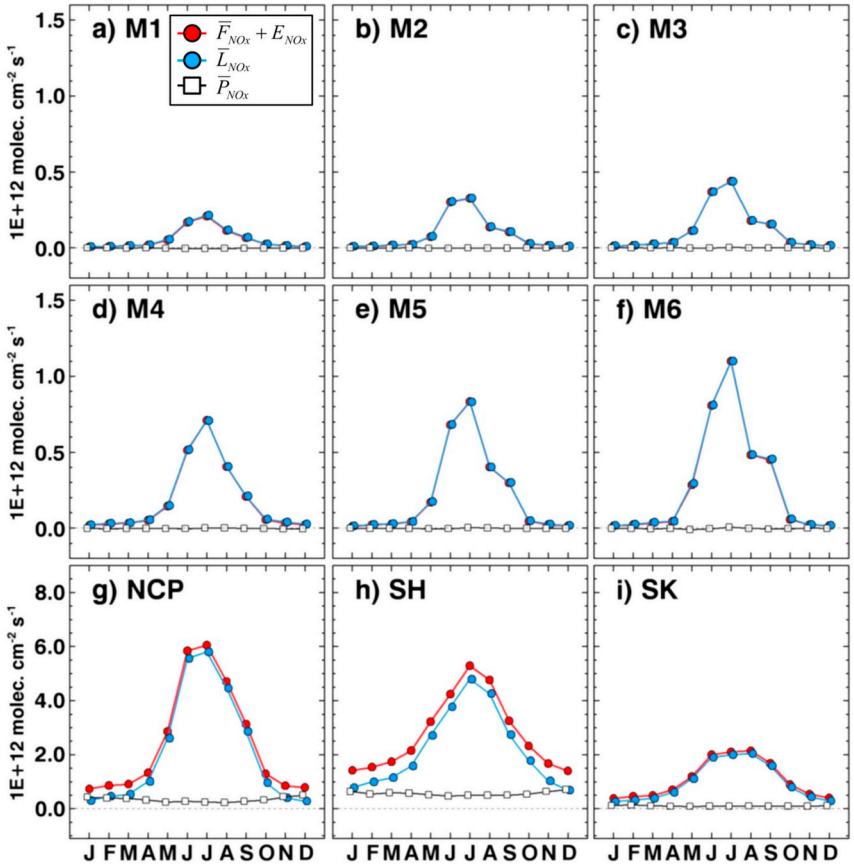

Fig. 6. Monthly variations of $\bar{F}_{NOx} + E_{NOx}$, $\bar{L}_{NOx}$, and $\bar{P}_{NOx}$ over the 9 analysis regions. All simulated data were extracted at 00–23 UTC. Panels of g), h), and i) have different scales in y-axis.

illustrated in Fig. 5, we added one more term of anthropogenic and soil NO_x emissions ($\bar{P}_{ENOx}$or E_{NOx}, molecules cm^{-2} s^{-1}) into the $\bar{P}_{NOx}$. This relation is shown by Eq. (4):

$$\begin{aligned}\bar{P}_{NOx} &= \bar{P}_{PANs} + \bar{P}_{RNO3} + \bar{P}_{hetero} + E_{NOx} \\ &= \bar{F}_{NOx} - \bar{L}_{NOx} + E_{NOx} \\ &= \int_{0}^{10km} (P_{NOx} - L_{NOx})dz + E_{NOx}\end{aligned} \quad (4)$$

Here, the transports of NO_x molecules between the grid cells can be assumed to be negligible due to relatively large analysis areas (shown in Fig. 1(b)) as well as short lifetimes of NO_x, particularly during summer. The entire budget was well balanced between the production rates ($\bar{F}_{NOx} + E_{NOx}$) and the chemical loss rates ($\bar{L}_{NOx}$) over the remote continental regions (M1 – M6) and the polluted regions (NCP, SH, and SK), as shown in Fig. 6. Based on these WRF-CMAQ model simulations, we inferred what the controlling factor(s) of the monthly NO_2 trends shown in continental background Asia are.

3.4. Budget analysis of $\bar{P}_{NOx}$

The monthly variations of Ω_{CMAQ} can be influenced by several parameters. One influential factor is the NO_x emitted from microbiological activity in soils, which is usually active during the warm seasons (van der A et al., 2006; Holland et al., 1999; Hudman et al., 2010). For example, Hudman et al. (2012) and Vinken et al. (2014) reported that in many parts of Kazakhstan, India, and Mongolia, the soil NO_x makes more than 50% contribution to the tropospheric NO_2 columns. The second factor would be the PAN decomposition. PANs can be transported from cold parts of the atmosphere to warm surface areas, and are then thermally decomposed into NO_2 (Singh and Hanst, 1981; Singh, 1987). In this way, PAN can be a source of NO_x in the remote regions (Val Martin et al., 2008; Kramer et al., 2015). On the other hand, NO_x can be destroyed through the reaction of NO_2+OH + M (here, M denotes the third body). This reaction is, in particular, active during warm seasons due to the high levels of OH. Another removal of atmospheric NO_x can be through the heterogeneous reactions of NO_3 and N_2O_5 radicals onto atmospheric aerosols, which are active during the nighttime (Brown and Stutz, 2012).

We analyzed the monthly budget of $\bar{P}_{NOx}$in Fig. 7 to find out the key processes for the monthly trends of Ω_{OMI} in the remote continental regions. We investigated four process rates defined in Sect. 3.3: i) NO_x emissions (E_{NOx} or $\bar{P}_{ENOx}$, denoted by white circles in Fig. 7); ii) $\bar{P}_{RNO3}$ (denoted by red squares); iii) $\bar{P}_{PANs}$ (denoted by blue triangles), and; iv) $\bar{P}_{hetero}$(denoted by yellow hexagons). As similar to those in Figs. 4 and 6, the budget analysis of $\bar{P}_{NOx}$ was also classified into three regional categories: i.e. i) the polluted regions (NCP, SH, and SK), ii) remote continental regions of southern Mongolia, and iii) remote continental regions of northern Mongolia. The positive or negative contributions of the four processes over polluted and remote continental regions were also presented in Fig. 8. The contributions from positive or negative contributors (processes, *i*) were separately calculated by Eq. (5). The positive and negative contributions range from 0 to 100 and from 0 to −100, respectively.

$$Contribution\ (\%) = \frac{\bar{P}_i}{\sum_{i=1}^{n} \bar{P}_i} \times 100 \quad (5)$$

3.4.1. Polluted regions: NCP, SH, and SK

For the polluted NCP, SH, and SK regions, E_{NOx} showed strong positive contributions while other parameters, $\bar{P}_{RNO3}$, $\bar{P}_{hetero}$, and $\bar{P}_{PANs}$ had negative values as shown in the panels g), h), and i) of Fig. 7. In terms of

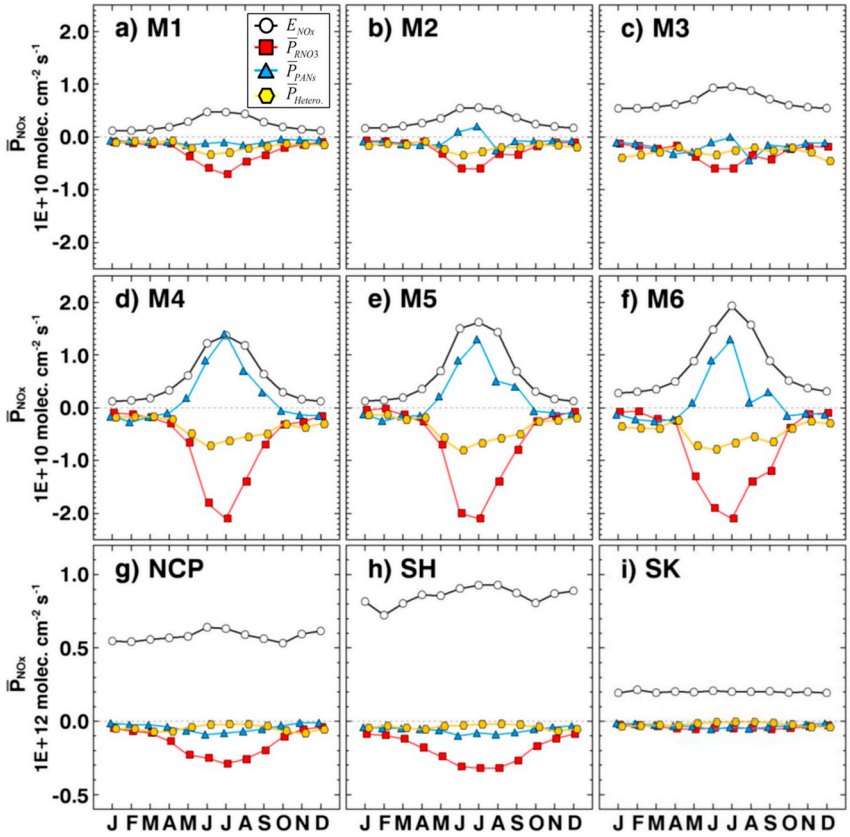

Fig. 7. Monthly budget of $\bar{P}_{NOx}$ over the 9 analysis regions. White circles, red squares, blue triangles, and yellow hexagons represent E_{NOx}, $\bar{P}_{RNO3}$, $\bar{P}_{PANs}$, and $\bar{P}_{Hetero}$, respectively. All simulated data were extracted from 00 to 23 UTC. Panels of g), h), and i) have different scales in y-axis. (For interpretation of the references to colour in this figure legend, the reader is referred to the Web version of this article.)

their magnitudes, E_{NOx} had the largest values for most of the months. The source of NO_x emissions considered in the CMAQ-model simulations was largely anthropogenic over these polluted areas. For example, the contribution of biological activity in the soil to the total NO_x emissions was only ~8% in most regions of the NCP area in July. The monthly variations of E_{NOx} were almost constant over the polluted regions. In the polluted regions, E_{NOx} was the only contributor of positive $\bar{P}_{NOx}$ (i.e. 100% shown in the panels g), h), and i) of Fig. 8). In terms of negative contributions, the largest values were found from $\bar{P}_{RNO3}$ (-42– -77% during the warm months). The formation rates ($\bar{F}_{RNO3}$) was 5–20% as fast as destruction rates ($\bar{L}_{RNO3}$), indicating negative contribution. The second largest contributor was $\bar{P}_{PANs}$ (-16– -50% during the warm months). The contribution of $\bar{P}_{hetero}$ were relatively small during the warm month. The negative contribution (or chemical loss) was mainly caused by the reaction of $NO_2 + OH + M$. From the analysis, it is likely to be concluded that the seasonal variation of Ω_{OMI} in the polluted areas (i.e. low Ω_{OMI} in summer and high Ω_{OMI} in winter) are primarily governed by active chemical loss through the reaction of $NO_2 + OH + M$ during the warm seasons.

3.4.2. Remote continental regions of southern Mongolia: M4, M5, and M6

In the remote continental regions of southern Mongolia (M4, M5, and M6), $\bar{P}_{RNO3}$ showed the largest negative values, which were similar to those in the polluted areas. However, as shown in Fig. 7d) and e), and f), these negative $\bar{P}_{RNO3}$ were completely offset by E_{NOx} and $\bar{P}_{PANs}$. The contribution of E_{NOx} to positive $\bar{P}_{NOx}$ ranges from 49 to 95% during warm seasons. In southern Mongolia, most of E_{NOx} were from microbiological activity in the soils (e.g. approximate 67–94% of total NO_x emission in the M4, M5, and M6 regions during the warm seasons). In addition, the magnitudes of $\bar{P}_{PANs}$in the polluted regions were negative and relatively small, whereas the contributions of $\bar{P}_{PANs}$ were positive and were large in remote southern Mongolia (5–51% contributions during the warm months). The contributions of $\bar{P}_{PANs}$were sometimes almost equivalent to those of E_{NOx} during the warm seasons. In other words, the thermal decomposition rates of PANs were faster than the PANs formation rates in these remote regions. Collectively, it indicated that the soil NO_x emissions and thermal decomposition of PANs are major sources of NO_x in the remote continental atmosphere. This would be the primary reason as to why CMAQ-calculated and OMI-observed NO_2 columns are high during the warm seasons and low during the cold seasons in the remote continental regions, Mongolia, unlike those in the polluted regions.

Fig. 8 shows the vertical distributions of monthly-averaged PAN mixing ratios over the remote northern and southern Mongolia and polluted regions. The surface concentrations of PAN were high in the polluted regions because the formation of PAN was more favorable than thermal decomposition of PAN due to sufficient amounts of precursors (NO_2 and $RCO(O)O_2$ radicals). On the contrary, the surface levels of PAN are lower in southern and northern Mongolia than those in the free troposphere, possibly because the thermal decomposition of PAN was favored during the warm seasons from June to August. Despite the active chemical losses of PAN during summer, some levels of PAN were found below ~600 hPa (see two red spots) over the M5 and M6 regions in Fig. 9e) and f). These two red spots were caused by medium-range transport of atmospheric PAN plumes from China to southern Mongolia by the southerly winds during summer. The transboundary transport events from Russia and Kazakhstan sometimes occur by the westerly winds in August. Such transboundary transport events can be found in the spatial analysis of PAN columns and wind patterns as shown in Fig. S3.

The contributions of $\bar{P}_{hetero}$to negative $\bar{P}_{NOx}$ range from −23% to −42% during the warm seasons and from −31% to −63% during the

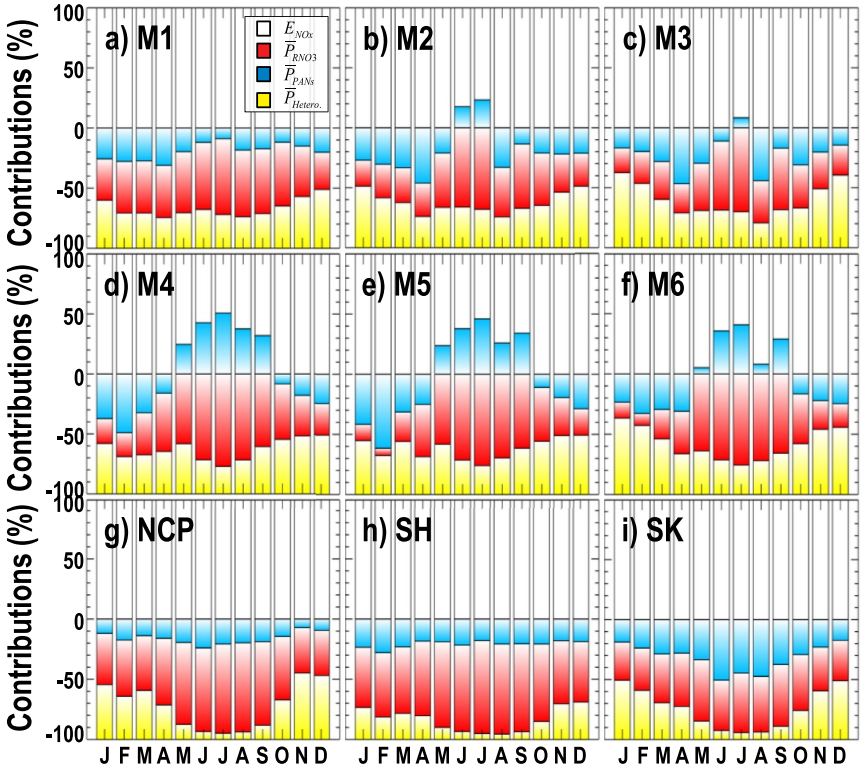

Fig. 8. Monthly positive and negative contributions of $\overline{P}_{NOx}$ over the 9 analysis regions. White, read, blue, and yellow boxes represent contributions from E_{NOx}, $\overline{P}_{RNO3}$, $\overline{P}_{PANs}$, and $\overline{P}_{Hetero}$, respectively. (For interpretation of the references to colour in this figure legend, the reader is referred to the Web version of this article.)

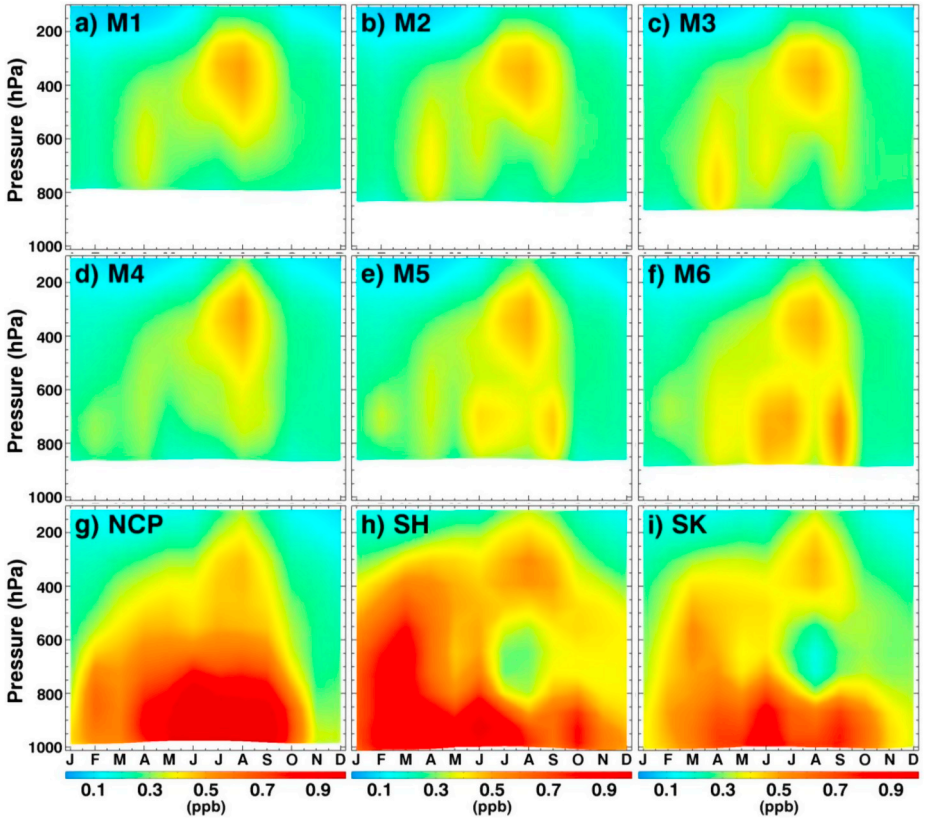

Fig. 9. Vertical distributions of monthly PAN concentrations (unit: ppb) from WRF-CMAQ model simulations. All simulated data were extracted from 00 to 23 UTC.

cold seasons. Despite higher contributions during the cold seasons, the magnitudes of $\bar{P}_{hetero}$were larger during the warm seasons. This was due to the fact that the high mixing ratios of NO_3 and N_2O_5 radicals were converted from high NO_2 mixing ratios during the warm seasons.

3.4.3. Remote continental regions of northern Mongolia: M1, M2, and M3

For the remote continental regions of northern Mongolia (M1, M2, and M3 regions), the discrepancy in Ω_{CMAQ} and Ω_{OMI} were relatively large as shown in Fig. 4a)–c), indicating that the bottom-up NO_x emissions used in the CMAQ-model simulations were possibly less accurate. The budget analysis was again carried out. According to the analysis, each component of $\bar{P}_{NOx}$ had relatively small values, but the monthly variations of the processes were similar to those in southern Mongolia as shown in (Fig. 7 d)–f)), which indicated that E_{NOx} and $\bar{P}_{PANs}$ are again major players in the high NO_2 columns during summer in northern Mongolia. However, the positive contributions from $\bar{P}_{PANs}$decreased significantly during the warm months, compared to those in southern Mongolia, as shown in Fig. 8.

4. Summary and conclusions

In this study, long-term OMI-observed NO_2 columns data from 2006 to 2015 were analyzed to understand the spatial distributions and temporal trends of tropospheric NO_2 columns in Mongolia (a remote continental region), where there is limited data from *in situ* ground measurements. From the seasonal trend analysis, we found the high variation of Ω_{OMI} during the warm seasons, and low Ω_{OMI} during the cold seasons over Mongolia. This is the exact opposite trend to that over the polluted areas in East Asia, such as the NCP, SH, and SK regions.

To determine the main factor controlling such monthly variations of NO_2 columns over Mongolia, we investigated the atmospheric chemical production and removal of NO_x and surface (soil) NO_x emission from the WRF-CMAQ simulations. In the analysis, we found that the monthly trends of the tropospheric NO_2 columns can be explained by $\bar{P}_{NOx}$(net columnar NO_x production rate) in the remote continental and polluted regions.

For the polluted regions, E_{NOx} was only positive and showed the largest values, followed by $\bar{P}_{RNO3}$ in terms of their magnitudes. Among the negative contributors, the contribution of $\bar{P}_{RNO3}$ to negative $\bar{P}_{NOx}$is the highest (−42 – -77% during the warm months), followed by $\bar{P}_{PANs}$(-16 – -50% during the warm months). From our analysis, the active chemical loss due to the reaction of $NO_2 + OH + M$ (which is the main channel of $\bar{P}_{RNO3}$) during summer is likely to cause the monthly cycles in Ω_{OMI} (lower Ω_{OMI} in summer and high Ω_{OMI} in winter) in the polluted regions. For the remote regions of (southern) Mongolia, $\bar{P}_{RNO3}$ have the largest (negative) fluxes in the magnitudes. However, these negative $\bar{P}_{RNO3}$ are almost completely offset by E_{NOx} and $\bar{P}_{PANs}$. Unlike the small contributions of $\bar{P}_{PANs}$ in the polluted areas, its contributions in southern Mongolia were positive and large during the warm summer (up to ~51% contribution). It was therefore concluded that the thermal decomposition of PANs can be one of major sources of NO_x in the remote continental atmosphere of (southern) Mongolia. In the analysis, it was found that atmospheric NO_2 was mainly from (soil) NO_x emissions and the thermal decomposition of PANs transported from China with southerly wind during summer. Collectively, the active thermal decomposition of PANs has important role for the high and low values of Ω_{CMAQ} and Ω_{OMI} in the remote continental regions of Mongolia during the warm and cold seasons, respectively. However, it would be further required that the model-estimated PAN mixing ratios in the troposphere over Mongolia are evaluated and validated for more accurate quantification in the budget of $\bar{P}_{NOx}$.

The analysis of satellite-derived data with chemistry-transport model results showed that the seasonal changes in tropospheric NO_2 columns are caused by the changes in the photochemical reaction(s) in the remote regions. Nevertheless, further data analysis of other remote continental regions (such as the western parts of China and central Asia) and higher-latitude regions (for example, Eurasia) are also needed. These further analyses will be helpful to facilitate a better understanding of atmospheric chemistry in such remote continental areas.

In addition, Geostationary Environment Monitoring Spectrometer (GEMS) sensor that will be launched in 2019 over Asia is expected to improve our capability to analyze the long-term trends of tropospheric NO_2 columns with a finer spatial and temporal resolution in many other regions in Asia. Also, additional studies should be conducted to investigate the potential impacts of permafrost soils around the Arctic circle on the variations of tropospheric NO_2 columns, caused by rapid changes in permafrost soils, due to on-going global warming.

Acknowledgements

This research was supported by National Research Foundation of Korea Grant from the Korean Government (MSIT; the Ministry of Science and ICT) (NRF-2016M1A5A1901769) (KOPRI-PN19081). This work was also supported by the National Strategic Project-Fine particle of the National Research Foundation of Korea, funded by the Ministry of Science and ICT (MSIT), the Ministry of Environment, and the Ministry of Health and Welfare (MOHW) (NRF- 2017M3D8A1092022). This work was also supported by Korea Ministry of Environment (MOE) as “Public Technology Program based on Environmental Policy (2017000160001)”. We would like to acknowledge the use of tropospheric NO_2 column data from TEMIS portal.

Appendix A. Supplementary data

Supplementary data to this article can be found online at https://doi.org/10.1016/j.atmosenv.2019.116817.

References

Batmunkh, T., Kim, Y.J., Jung, J.S., Park, K., Tumendemberel, B., 2013. Chemical characteristic of fine particulate matters measured during severe winter haze events in Ulaanbaatar, Mongolia. J. Air Waste Manag. Assoc. 63, 659–670.

Binkowski, F.S., Rosell, S.J., 2003. Models-3 Community Multi-scale Air Quality (CMAQ) model aerosol components: 1. model description. J. Geophys. Res. 108 (D6), 4183. https://doi.org/10.1029/2001JD001409.

Boersma, K.F., Jacob, D.J., Trainic, M., Rudich, Y., DeSmedt, I., Dirksen, R., Eskes, H.J., 2009. Validation of urban NO_2 concentrations and their diurnal and seasonal variations observed from the SCIAMACHY and OMI sensors using in situ surface measurements in Israeli cities. Atmos. Chem. Phys. 9, 3867–3879.

Boersma, K.F., Eskes, H.J., Dirksen, R.J., van der A, R.J., Veefkind, J.P., Stammes, P., Huijnen, V., Kleipool, Q.L., Sneep, M., Claas, J., Leitão, J., Richter, A., Zhou, Y., Brunner, D., 2011a. An improved tropospheric NO_2 column retrieval algorithm for the Ozone monitoring instrument. Atmos. Meas. Tech. 4 1905–28.

Boersma, K.F., Braak, R., van der A, R.J., 2011b. Dutch OMI NO_2 (DOMINO) Data Product v2.0 HE5 Data File User Manual. http://www.temis.nl/airpollution/no2.html.

Boersma, K.F., Vinken, G.C.M., Tournadre, J., 2015. Ships going slow in reducing their NO_x emissions: changes in 2005-2012 ship exhaust inferred from satellite measurements over Europe. Environ. Res. Lett. 10, 074007.

Brown, S.S., Stutz, J., 2012. Nighttime radical observations and chemistry. Chem. Soc. Rev. 41, 6405–6447.

Byun, D.W., Schere, K.L., 2006. Review of the governing equations, computational algorithm, and other components of the Models-3 Community Multi-scale Air Quality (CMAQ) modeling system. Appl. Mech. Rev. 59, 51–77.

Carter, W.P.L., 2000. Implementation of the SAPRC-99 Chemical Mechanism into the Models-3 Framework. United States Environmental Protection Agency.

Chang, J.S., Brost, R.A., Isaksen, I.S.A., Madronich, S., Middleton, P., Stockwell, W.R., Walcek, F.S., 1987. A three-dimensional eulerian acid deposition model: physical concepts and formulation. J. Geophys. Res. 92 (D12), 14681–14700.

Choi, Y., Souri, A.H., 2015. Chemical condition and surface ozone in large cities of Texas during the last decade: observational evidence from OMI, CAMS, and model analysis. Remote Sens. Environ. 168, 90–101.

Darmenov, A., da Silva, A.M., 2013. The Quick Fire Emission Dataset (QFED)-Documentation of Versions 2.1, 2.2 and 2.4, vol. 32 NASA TM-2013-104606. http://gamo.gsfc.nasa.gov/pubs/tm/ 183.

Davis, J.M., Bhave, P.V., Foley, K.M., 2008. Parameterization of N_2O_5 reaction probabilities on the surface of particles containing ammonium, sulfate, and nitrate. Atmos. Chem. Phys. 8, 5295–5311. https://doi.org/10.5194/acp-8-5295-2008.

Davy, P.K., Gunchin, G., Markwitz, A., Trompetter, W.J., Barry, B.J., Shagjjamba, D., Lodysamba, S., 2011. Air particulate matter pollution in Ulaanbaatar, Mongolia: determination of composition, source contributions and source locations. Atmos. Pollut. Res. 2, 126–137.

de Foy, B., Lu, Z., Streets, D.G., 2016. Impacts of control strategies, the Great Recession

and weekday variations on NO_2 columns above North American cities. Atmos. Environ. 138, 74–86.
Dudhia, J., 1989. Numerical study of convection observed during the winter monsoon experiment using a mesoscale two-dimensional model. J. Atmos. Sci. 46, 3077–3107.
Duncan, B.N., Lamsal, L.N., Thompson, A.M., Yoshida, Y., Lu, Z., Streets, D.G., Hurwitz, M.M., Pickering, K.E., 2016. A space-based, high-resolution view of notable changes in urban NO_x pollution around the world (2005-2014). J. Geophys. Res. 121, 976–996.
EANET, 2012. Data Report 2010. Network Center for EANET, ACAP, Japan.
Emmons, L.K., Walters, S., Hess, P.G., Lamarque, J.-F., Pfister, G.G., Fillmore, D., Granier, C., Guenther, A., Kinnison, D., Laepple, T., Orlando, J., Tie, X., Tyndall, G., Wiedinmyer, C., Baughcum, S.L., Kloster, S., 2010. Description and evaluation of the model for ozone and related chemical Tracers, version 4 (MOZART-4), geosci. Model Dev 3, 43–67.
Environmental Protection Agency, 1999. Science Algorithms of the EPA Models-3 Community Multiscale Air Quality (CMAQ) Modeling System, EPA-600/R-99/030. Washington, D. C., 14-1 – 14-7.
Evans, M.J., Jacob, D.J., 2005. Impact of new laboratory studies of N_2O_5 hydrolysis on global model budgets of tropospheric nitrogen oxides, ozone, and OH. Geophys. Res. Lett. 32, L09813. https://doi.org/10.1029/2005GL022469.
Exner, M., Herrmann, H., Zellner, R., 1994. Rate constants for the reactions of the NO_3 radical with $HCOOH/HCOO^-$ and $CH3COOH/CH3COO^-$ in aqueous solution between 278 and 328K. J. Atmos. Chem. 18, 359–378.
Han, K.M., Lee, C.K., Lee, J., Kim, J., Song, C.H., 2011. A comparison study between model-predicted and OMI-retrieved NO_2 columns over the Korean peninsula, Atmos. Environ. Times 45, 2962–2971.
Han, K.M., Lee, S., Chang, L.S., Song, C.H., 2015. A comparison study between CMAQ-simulated and OMI-retrieved NO_2 columns over East Asia for evaluation of NO_x emission fluxes of INTEX-B, CAPSS, and REAS inventories. Atmos. Chem. Phys. 15, 1913–1938.
Holland, E., Dentener, F.J., Braswell, B.H., Sulzman, J.M., 1999. Contemporary and pre-industrial global reactive nitrogen budgets. Biogeochemistry 46, 7–43.
Hong, S.Y., Noh, Y., Dudhia, J., 2006. A new vertical diffusion package with and explicit treatment of entrainment processes. Mon. Weather Rev. 134, 2318–2341. https://doi.org/10.1175/MWR3199.1.
Huang, Y., Luvsan, M., Gombojav, E., Ochir, C., Bulgan, J., Chan, C., 2013. Land use patterns and SO_2 and NO_2 pollution in Ulaanbaatar, Mongolia. Environ. Res. 124, 1–6.
Hudman, R.C., Russell, A.R., Valin, L.C., Cohen, R.C., 2010. Interannual variability in soil nitric oxide emissions over the United States as viewed from space. Atmos. Chem. Phys. 10, 9943–9952.
Hudman, R.C., Moore, N.E., Mebust, A.K., Martin, R.V., Russell, A.R., Valin, L.C., Cohen, R.C., 2012. Steps towards a mechanistic model of global soil nitric oxide emissions: implementation and space based-constraints. Atmos. Chem. Phys. 12, 7779–7795.
Huijnen, V., Eskes, H.J., Poupkou, A., Elbern, H., Boersma, K.F., Foret, G., Sofiev, M., Valdebenito, A., Flemming, J., Stein, O., Gross, A., Robertson, L., D'Isidoro, M., Kioutsioukis, I., Friese, E., Amstrup, B., Bergstrom, R., Strunk, A., Vira, J., Zyryanov, D., Maurizi, A., Melas, D., Peuch, V.-H., Zerefos, C., 2010. Comparison of OMI NO_2 tropospheric columns with an ensemble of global and European regional air quality models. Atmos. Chem. Phys. 10, 3273–3296.
Irie, H., Boersma, K.F., Kanaya, Y., Takashima, H., Pan, X., Wang, Z.F., 2012. Quantitative bias estimates for tropospheric NO_2 columns retrieved from SCIAMACHY, OMI, and GOME-2 using a common standard for East Asia. Atmos. Meas. Tech. 5, 2403–2411.
Jacob, D.J., 2000. Heterogeneous chemistry and tropospheric ozone. Atmos. Environ. 34, 2131–2159.
Jaeglé, L.R., Martin, R.V., Chance, K., Steinberger, L., Kurosu, T.P., Jacob, D.J., Modi, A.I., Yoboué, V., Sigha-Nkamdjou, L., Galy-Lacaux, C., 2004. Satellite mapping of rain-induced nitric oxide emissions from soils. J. Geophys. Res. 109, D21310. https://doi.org/10.1029/2004JD004787.
Jin, J., Ma, J., Lin, W., Zhao, H., Shaiganfar, R., Beirle, S., Wagner, T., 2016. MAX-DOAS measurements and satellite validation of tropospheric NO_2 and SO_2 vertical column densities at a rural site of North China, Atmos. Environ. Times 133, 12–25.
Kramer, L.J., Helmig, D., Burkhart, J.E., Stohl, A., Oltmans, S., Honrath, R.E., 2015. Seasonal variability of atmospheric nitrogen oxides and non-methane hydrocarbons at the GEOSummit station, Greenland. Atmos. Chem. Phys. 15, 6827–6849.
Krotkov, N.A., McLinden, C.A., Li, C., Lamsal, L.N., Celarier, E.A., Marchenko, S.V., Swartz, W.H., Bucsela, E.J., Joiner, J., Duncan, B.N., Boersma, K.F., Veefkind, J.P., Levelt, P.F., Fioletov, V.E., Dickerson, R.R., He, H., Lu, Z., Streets, D.G., 2016. Aura OMI observations of regional SO_2 and NO_2 pollution changes from 2005 to 2015. Atmos. Chem. Phys. 16, 4605–4629.
Kurokawa, J., Ohara, T., Morikawa, T., Hanayama, S., Janssens-Maenhout, G., Fukui, T., Kawashima, K., Akimoto, H., 2013. Emissions of air pollutants and greenhouse gases over Asian regions during 2000–2008: regional Emission inventory in ASia (REAS) version 2. Atmos. Chem. Phys. 13, 11019–11058.
Lamsal, L.N., Martin, R.V., van Donkelaar, A., Celarier, E.A., Bucsela, E.J., Boersma, K.F., Luo, R.D.C., Wang, Y., 2010. Indirect validation of tropospheric nitrogen dioxide retrieved from the OMI satellite instrument: insight into the seasonal variation of nitrogen oxides at northern midlatitudes. J. Geophys. Res. 115, D05302. https://doi.org/10.1029/2009JD013351.
Lamsal, L.N., Krotkov, N.A., Celarier, E.A., Swartz, W.H., Pickering, K.E., Bucsela, E.J., Gleason, J.F., Martin, R.V., Philip, S., Irie, H., Cede, A., Herman, J., Weinheimer, A., Szykman, J.J., Knepp, T.N., 2014. Evaluation of OMI operational standard NO_2 column retrievals using in situ and surface-based NO_2 observations. Atmos. Chem. Phys. 14, 11587–11609.
Levelt, P.F., Hilsenrath, E., Leppelmeier, G., van den Oord, G., Bhartia, P.K., Tamminen, J., de Haan, J., Veefkind, J., 2006. Science objectives of the ozone monitoring instrument. IEEE Trans. Geosci. Remote Sens. 44, 1199–1208.
Li, M., Zhang, Q., Kurokawa, J.-I., Woo, J.-H., He, K., Lu, Z., Ohara, T., Song, Y., Streets, D.G., Carmichael, G.R., Cheng, Y., Hong, C., Huo, H., Jiang, X., Kang, S., Liu, F., Su, H., Zheng, B., 2017. MIX: a mosaic Asian anthropogenic emission inventory under the international collaboration framework of the MICS-Asia and HTAP. Atmos. Chem. Phys. 17, 935–963.
Lin, J.-T., Martin, R.V., Boersma, K.F., Sneep, M., Stammes, P., Spurr, R., Wang, P., Van Roozendael, M., Clémer, K., Irie, H., 2014. Retrieving tropospheric nitrogen dioxide from the Ozone Monitoring Instrument: effects of aerosols, surface reflectance anisotropy, and vertical profile of nitrogen dioxide. Atmos. Chem. Phys. 14, 1441–1461.
Mendolia, D., D'Souza, R.J.C., Evans, G.J., Brook, J., 2013. Comparison of tropospheric NO_2 vertical columns in an urban environment using satellite, multi-axis differential optical absorption spectroscopy, and in situ measurements. Atmos. Meas. Tech. 6, 2907–2924.
Mlawer, E.J., Taubman, S.J., Brown, P.D., Iacono, M.J., Clough, S.A., 1997. Radiative transfer for inhomogenous atmosphere: RRTM, a validated correlated-k model for the longwave. J. Geophys. Res. 102 (D14), 16663–16682.
Richter, A., Burrow, J.P., Nüß, H., Granier, C., Niemeier, U., 2005. Increase in tropospheric nitrogen dioxide over China observed from space. Nature 437, 129–132.
Riemer, N., Vogel, H., Vogel, B., Schell, B., Ackermann, I., Kessler, C., Hass, H., 2003. Impact of the heterogeneous hydrolysis of N_2O_5 on chemistry and nitrate aerosol formation in the lower troposphere under photosmog conditions. J. Geophys. Res. 108, 4144. https://doi.org/10.1029/2002JD002436.
Schneider, P., Lahoz, W.A., van der A, R., 2015. Recent satellite-based trends of tropospheric nitrogen dioxide over large urban agglomerations worldwide. Atmos. Chem. Phys. 15, 1205–1220.
Schwartz, S.E., 1986. In: Jaeschke, W. (Ed.), Mass Transport Considerations Pertinent to Aqueousphase Reactions of Gases in Liquid-Water Clouds, Chemistry of Multiphase Atmospheric System. Springer-Verlag, Berlin, pp. 415–471.
Shaiganfar, R., Beirle, S., Petetin, H., Zhang, Q., Beekmann, M., Wagner, T., 2015. New concepts for the comparison of tropospheric NO_2 column densities derived from car-MAX-DOAS observations, OMI satellite observations and the regional model CHIMERE during two MEGAPOLI campaigns in Paris 2009/10. Atmos. Meas. Tech. 8, 2827–2852.
Sharkhuu, N., 2003. Recent changes in permafrost in Mongolia. In: In: Phillips, M., Springman, S.M., Arenson, L.U. (Eds.), Proceedings of the 8th International Conference on Permafrost, July 20–25, 2003, Zurich, Lisee, A.A. Balkema, vols. 1029–1034.
Sindelarova, K., Granier, C., Bouarar, I., Guenther, A., Tilmes, S., Stavrakou, T., Müller, J.-F., Kuhn, U., Stefani, P., Knorr, W., 2014. Global data set of biogenic VOC emissions calculated by the MEGAN model over the last 30 years. Atmos. Chem. Phys. 14, 9317–9341. https://doi.org/10.5194/acp-14-9317-2014.
Skamarock, W.C., Klemp, J.B., Dudhia, J., Gill, D.O., Barker, D.M., Duda, M.G., Huang, X.Y., Wang, W., Powers, J.G., 2008. A Description of the Advanced Research WRF Version 3, NCAR Technical Note, NCAR/TN-475+STR, vol. 113 NCAR, Boulder, CO, USA.
Singh, H.B., Hanst, P.L., 1981. Peroxyacetyl nitrate (PAN) in the unpolluted atmosphere: an important reservoir for nitrogen oxides. Geophys. Res. Lett. 8, 941–944.
Singh, H.B., 1987. Reactive nitrogen in the troposphere-chemistry and transport of NO_x and PAN. Environ. Sci. Technol. 21, 320–327.
Val Martin, M., Honrath, R.E., Owen, R.C., Li, Q.B., 2008. Seasonal variation of nitrogen oxides in the central North Atlantic lower free troposphere. J. Geophys. Res. 113, D17307. https://doi.org/10.1029/2007JD009688.
van der A, R.J., Peters, D.H.M.U., Eskes, E., Boersma, K.F., Van Roozendael, M., 2006. Detection of the trend and seasonal variation in tropospheric NO_2 over China. J. Geophys. Res. 111, D12317. https://doi.org/10.1029/2005JD006594.
van der A, R.J., Eskes, H.J., Boersma, K.F., van Noije, T.P.C., Van Roozendael, M., De Smedt, I., Peters, D.H.M.U., Meijer, E.W., 2008. Trends, seasonal variability and dominant NOx source derived from a ten year record of NO_2 measured from space. J. Geophys. Res. 113, D04302. https://doi.org/10.1029/2007JD009021.
van Noije, T.P.C., Eskes, H.J., Dentener, F.J., Stevenson, D.S., Ellingsen, K., Schultz, M.G., Wild, O., Amann, M., Atherton, C.S., Bergmann, D.J., Bey, I., Boersma, K.F., Butler, T., Cofala, J., Drevet, J., Fiore, A.M., Gauss, M., Hauglustaine, D.A., Horowitz, L.W., Isaksen, I.S.A., Krol, M.C., Lamarque, J.-F., Lawrence, M.G., Martin, R.V., Montanaro, V., Müller, J.-F., Pitari, G., Prather, M.J., Pyle, J.A., Richter, A., Rodriguez, J.M., Savage, N.H., Strahan, S.E., Sudo, K., Szopa, S., van Roozendael, M., 2006. Multi-model ensemble simulations of tropospheric NO_2 compared with GOME retrievals for the year 2000. Atmos. Chem. Phys. 6, 2943–2979.
Vinken, G.C.M., Boersma, K.F., Maasakkers, J.D., Adon, M., Martin, R.V., 2014. Worldwide biogenic soil NO_x emissions inferred from OMI NO_2 observations. Atmos. Chem. Phys. 14, 10363–10381.
Willmott, C.J., 1981. On the validation of models. Phys. Geogr. 2, 184–194.
World Bank, 2009. Air Pollution in Ulaanbaatar: Initial Assessments of Current Situation and Effects of Abatement Measures. The World Bank), Washington DC.
World Health Organization, 2014. Ambient (Outdoor) Air Pollution Database 2014, by Country and City. http://www.who.int/phe/health_topics/outdoorair/databases/cities-2014/en/.
World Health Organization, 2016. Ambient Air Pollution: A Global Assessment of Exposure and Burden of Disease Report, vol. 131.
Yienger, J.J., Levy II, H., 1995. Empirical model of global soil-biogenic NO_x emissions. J. Geophys. Res. 100, 11447–11464.